Engineering Structures 316 (2024) 118556

Contents lists available at ScienceDirect

Engineering Structures

journal homepage: www.elsevier.com/locate/engstruct

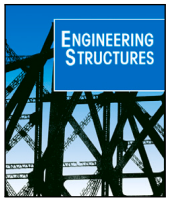

Load-bearing capacity of slender dowel-type fasteners in Timber-Concrete Composite connections

Johan Pyykkö [a,b,*], Staffan Svensson [a]

[a] University of Borås, Faculty of Textiles, Engineering and Business, Allégatan 1, 501 90 Borås, Sweden
[b] Uppsala University, Division of Applied Mechanics, Ångström Laboratory, Uppsala, Sweden

ARTICLE INFO

Keywords:
Timber-Concrete Composite connections
Mechanical connections
Deformed state equilibrium
Plastic hinge
Slender fasteners

ABSTRACT

Load-bearing capacity of slender dowel-type fasteners of round ring-shank nails and U-shaped connectors (U-conn:s) of square cross-sectional nail thread used as connections in Timber-Concrete Composite structures have been studied, experimentally and with two different theoretical models. Tensile strength and withdrawal capacity of fasteners and embedment strength of timber were tested and evaluated. The parameters were used for calculation of the plastic hinge location in the fastener on the timber side and the load-bearing capacity of the connections. For this, both the European Yield Model known from the Eurocode 5, as well as a model where the load-bearing capacity is determined from mechanical equilibrium of fasteners in deformed state were used. Double shear push-out tests were carried out to determine the load-carrying capacity of the connections. The calculated values are compared to the experimental results. The models showed similar results for the U-conn:s regarding both plastic hinge location and load-bearing capacity. For the nails, all models show good correlation with experimental values, however, the model derived from the deformed state predicted both the plastic hinge location and the load-carrying capacity more accurately.

1. Introduction

As a part of the increasing interest in multi-storey buildings with timber structures, interest in Timber-Concrete Composite (TCC) floor systems has increased. In comparison to traditional timber-based floor systems, TCC structures have an increased load-bearing capacity as well as increased stiffness [1]. Furthermore, greater damping, stiffness and mass is beneficial for sound isolation [2,3], floor vibrations [4–7] and structural stabilisation [1]. In addition, the reduced amount of concrete used enables for savings in production costs and time [8] as well as in decrease of the environmental impact [9,10].

To fully utilise the mechanical properties of the materials and allow for load-sharing between the components of TCC elements, the connection between components is of crucial importance. Thus, one of the most important properties of TCC structures is the behaviour and load-bearing capacity of the internal connection. There are different connection systems, described in e.g. [8,11,12]. One of the most used connections systems is dowel-type fasteners, and the load-bearing capacity is usually determined using models for timber–timber connections [13]. To assess the load-bearing capacity of dowelled and bolted timber connections the well-known Johansen model was developed in the 1940s [14], taking plastic resistance of steel dowel bending and wood into consideration. When developing the model, tests were made also on nailed connections. These results were published by Larsen [15], although similar assumptions were used to assess nailed connections by Möller [16]. While antimetry, i.e. same embedment strength in the connected timber sections, was assumed in [14], influence of different embedment strengths of timber sections was included in [15–17]. In [15] "secondary contributions owing to axial forces", i.e. tension in nail and friction between wood surfaces, often referred to as rope-effect, was included. The aforementioned Johansen theory, with extensions due to rope-effect [15,18], is commonly known as the European Yield Model (EYM). In analogy with the work of Johansen, dowels and bolts embedded in concrete were studied in [19]. In many recent studies of TCC connections, numerical models have been used both for connections [20,21], as well as for structural elements [22,23].

The approach of Johansen is mechanically traceable, based on equilibrium of forces, geometric and material parameters. Although mechanical purity is reduced when the rope-effect is considered [24], the EYM offers an efficient and straightforward method to calculate the load-bearing capacity of fasteners, and in Eurocode 5 it is proposed for both timber–timber [25] and timber-concrete [26] connections. The EYM was used for TCC connections in [27], and models obtained with similar approach in [13], using different assumptions for the concrete embedment. The models were derived from the undeformed

* Corresponding author at: University of Borås, Faculty of Textiles, Engineering and Business, Allégatan 1, 501 90 Borås, Sweden.
E-mail address: johan.pyykko@hb.se (J. Pyykkö).

https://doi.org/10.1016/j.engstruct.2024.118556
Received 7 March 2024; Received in revised form 4 June 2024; Accepted 1 July 2024
Available online 14 July 2024

fastener configuration showing good correlation with experimental values, but in most cases tended to underestimate the load-bearing capacity. Models derived from mechanical equilibrium are also used for TCC connections with screws, and if the screw has an inclination to the shear surface between materials the axial force can be directly considered in the model derivation [28–30]. A similar approach to Johansen's is also used in [31], where a deformation controlled connection design is proposed, and models derived from mechanical equilibrium have also been used to simulate load-slip behaviour of fasteners [32]. In such applications, the positions of the plastic hinges are decisive [33].

The aforementioned models are using equilibrium in the undeformed state to determine the load-bearing capacity of the fasteners. It is shown in [34,35] that a better estimation of the load-bearing capacity for timber–timber joints is reached when the nail is studied in the deformed state, especially for slender nails with high withdrawal capacity. This is also shown for TCC connections in [36]. Furthermore, in [36] it is also shown that a better prediction of the plastic hinge location can be obtained from equilibrium in the deformed state.

In this paper, firstly the models to describe the load-bearing capacity from mechanical equilibrium in both undeformed and deformed configuration are derived for TCC connections, and the model in the deformed state is developed with a function taking the axial load influence on the yield moment into consideration. Secondly, the important model material parameters are tested. Thirdly, push-out tests on TCC connections are performed. The results from all tests are presented and discussed. The tested material parameters are used in the theoretical models to determine the hinge location and load-bearing capacity of the TCC connections. Lastly, the theoretical values are compared to the push-out tests and conclusions are drawn.

2. Theory and calculations

When determining the load-bearing capacity, the wood and concrete embedments are assumed to behave as ideal plastic materials with the embedding strengths $f_{h,t}$ and $f_{h,c}$, respectively, while the steel fastener is assumed to have the yield moment M_y. Furthermore, the fastener is assumed to have sufficient penetration depth on each side of the joint, so that plastic hinges can develop in the fastener in both connected members. The mechanical state beyond the plastic hinges are self-equilibrating and are therefore not contributing to the load-bearing capacity. The fastener is assumed to be fully anchored on the concrete side, so the axial capacity of the fastener in timber will be decisive.

In Fig. 1, fasteners with load assumptions are depicted in undeformed (left) and deformed states (right). In the figure, M_y is the fastener yield moment, q_c and q_t are the uniformly distributed embedment-loads while x_c and x_t are the distances from the connection's shear plane to the fastener's plastic hinges, on the concrete and timber side, respectively. Furthermore, q_{ax} is the axial load on the fastener on the timber side, l_t is the depth of penetration in the timber, and φ is the bending angle of the deformed fastener. Since the ultimate load-bearing capacity of the connection is sought, the loads on the fastener are determined from the embedment strengths of timber $f_{h,t}$ and concrete $f_{h,c}$, the withdrawal strength parameter f_{ax}, and the width d of the fastener as;

$$q_t = d \cdot f_{h,t} \tag{1}$$

$$q_c = d \cdot f_{h,c} \tag{2}$$

$$q_{ax} = d \cdot f_{ax}. \tag{3}$$

In the expressions, the width d is the diameter if round or the side length if square cross-sectional fasteners are used, cf. [15].

2.1. Load-bearing capacity in undeformed state

With the loads presented in (1) to (3), the moment equilibrium about the left hinge of the undeformed fastener in Fig. 1 is;

$$\circlearrowleft : 2M_y + q_c x_c \frac{x_c}{2} - q_t x_t \left(x_c + \frac{x_t}{2}\right) = 0. \tag{4}$$

By using force equilibrium perpendicular to the fastener axis between the plastic hinges, the distance from the connection's shear plane to the plastic hinge on the concrete side can be solved from (4) as;

$$x_t = \sqrt{\frac{4M_y}{q_t(1+\beta)}}, \tag{5}$$

where $\beta = q_t/q_c$.

The ultimate force can now be expressed as;

$$F_{undef.} = q_t \cdot x_t = \sqrt{\frac{4M_y q_t}{1+\beta}}. \tag{6}$$

The derived expression can be recognised in equation 8.6 (f) from Eurocode 5 [25]. In Eurocode 5, however, a correction accounting for the derivation of design values from characteristic values as described in [37] is done, which is omitted here. Furthermore, in the Eurocode 5 an additional capacity due to axial force in the fastener and friction is considered (rope-effect). The contribution from the rope-effect is set to 25% of the axial capacity, with limitations depending on the fastener type [25,37]. Thus, the load-bearing capacity according to EYM as defined in Eurocode 5 can be expressed as;

$$F_{EYM} = F_{undef.} + \min\left(0.25 \cdot F_{ax,EYM}; A \cdot F_{undef.}\right) \tag{7}$$

wherein $F_{ax,EYM}$ is the axial capacity, and A is a limiting constant (see [37]). The axial capacity of the fastener on the timber side is determined as;

$$F_{ax,EYM} = q_{ax} l_w \tag{8}$$

wherein the withdrawal length l_w is the whole penetration depth l_t for smooth nails and the length of the ringed part for ring-shank nails.

2.2. Load-bearing capacity in deformed state

The deformed fastener is idealised in such a way that the bending deformation is localised to one single cross-section. The bending deformation is described by the angle φ, as shown in the right illustration of Fig. 1. The moment equilibrium about the left hinge can be written as;

$$\circlearrowleft : 2M_y + q_c x_c \frac{x_c}{2} - q_t x_t \left(x_c + \frac{x_t}{2}\right) + F_{ax,def}\left(x_c + x_t\right)\sin\varphi = 0, \tag{9}$$

where $F_{ax,def}$ is the axial capacity of the fasteners (8), where withdrawal length is taken inside the hinge and considering the ringed part for ring-shank nails. With same force relations as in (5), the distance x_t between the connection shear plane and the plastic hinge is solved from (9) as;

$$x_t = \frac{F_{ax,def}\sin\varphi}{q_t} + \sqrt{\left(\frac{F_{ax,def}\sin\varphi}{q_t}\right)^2 + \frac{4M_y}{q_t(1+\beta)}}. \tag{10}$$

As a consequence of axial constraint of the deforming fastener, normal force develops as tension in the fastener and thus compression on the shear plane. This force is identified as the sum of anchorage force $F_{ax,def}$ and components of the embedment load and the friction force between fastener and wood caused by it. Furthermore, this force contributes to the load-bearing capacity due to friction in the shear plane as;

$$F_{fr} = \left(F_{ax,def} + q_t x_t \mu_{ws}\cos\varphi - q_t x_t \sin\varphi\right)\mu_{wc}. \tag{11}$$

The ultimate force in the shear plane can be determined by adding the vertical components of the lateral load on the fastener on the timber

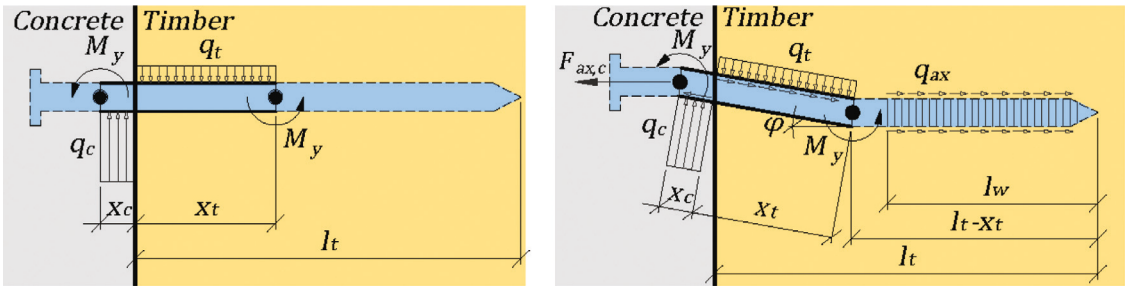

Fig. 1. Fastener in undeformed (left) and deformed (right) states. In the figure, the shear plane of the connection, i.e. the interface between concrete and timber, is illustrated by a vertical line. Furthermore, the lateral and axial loads on the fastener as well as the plastic hinge location in each material is indicated.

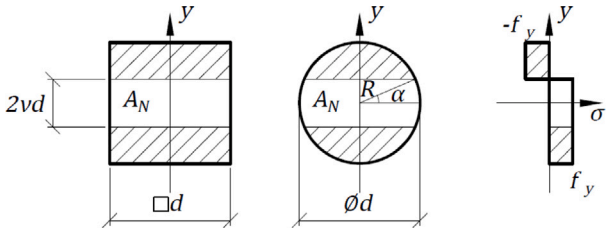

Fig. 2. The quadratic and circular cross-sections stressed in combined bending and tension, alongside the stress distribution when the full plastic strength is reached.

side, the friction between fastener and timber, and the friction force from Eq. (11). Thus, the capacity of the connection is:

$$F_{DEF} = q_t x_t \left(\cos\varphi\left(1+\mu_{ws}\mu_{wc}\right)+\sin\varphi\left(\mu_{ws}-\mu_{wc}\right)\right)+F_{ax,def}\mu_{wc}. \quad (12)$$

In the expressions, μ_{ws} and μ_{wc} are friction coefficients between wood-steel and wood-concrete, respectively. The derived equation is also recognised in [35].

The withdrawal force, as well as the frictional forces, are reactions activated by the shear of the plane between the timber and concrete. The axial force in the hinge is limited by the withdrawal capacity of the fastener (8), and can of course not exceed the tensile capacity of the steel.

2.2.1. Influence of axial force on yield moment

Different approaches to calculate the yield moment are discussed in e.g. [38], here however the theoretical state of fully plasticised cross-sections is used. In the subsequent calculations, the yield strength is used to determine the yield moment for the quadratic and circular cross-section, respectively, as;

$$M_{y,quadratic} = f_y \frac{d^3}{4} \quad (13)$$

$$M_{y,circular} = f_y \frac{d^3}{6}. \quad (14)$$

These yield moments are used for the calculations in the undeformed state. For the equations derived from the deformed state, however, the presence of a tensile normal force will reduce the yield moment of the cross-section, see e.g. [39]. This reduction is determined by studying the stress state in a cross-section loaded in bending and tension when the yield stress is reached within the entire cross-section. The quadratic and circular cross-sections are depicted alongside the assumed stress distribution in Fig. 2.

By assuming yield stress f_y in the entire quadratic cross-section depicted in Fig. 2, the area A_N required for a certain normal force N can be written as

$$\frac{N}{f_y} = A_N = 2vd^2 \quad (15)$$

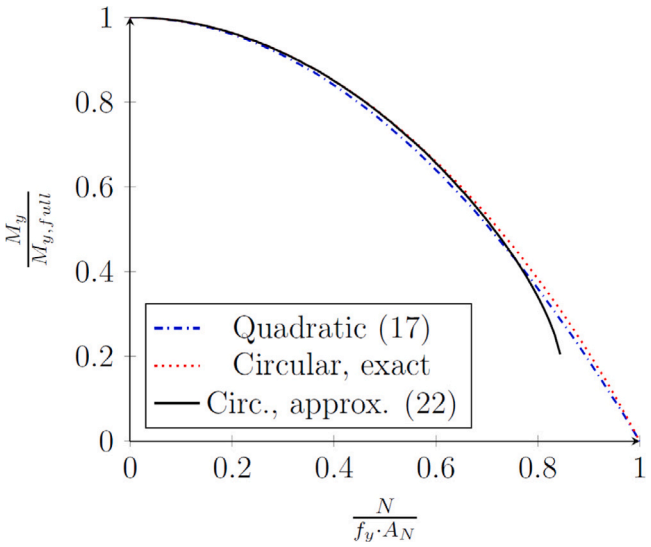

Fig. 3. Interaction diagram of bending moment and axial force for quadratic and circular cross-sections at full plastic state. For the bending moments, $M_{y,full}$ represents the yield moments obtained with (13) and (14) for the quadratic and circular cross-sections, respectively.

Furthermore, from the definition of plastic bending stress, the plastic section modulus Z for the hatched part of the quadratic cross-section in Fig. 2 can be determined as

$$\frac{M_y}{f_y} = Z = 2\int_{vd}^{\frac{d}{2}} y d\,\mathrm{d}y = d^3\left(\frac{1}{4}-v^2\right). \quad (16)$$

By insertion of (15) in (16), the moment as a function of normal force can be written as

$$M_y(N) = \frac{f_y d^3}{4}\left(1-\left(\frac{N}{d^2 f_y}\right)^2\right). \quad (17)$$

This expression is normalised against the full yield moment derived with (13) and is plotted in Fig. 3.

Likewise, for the circular cross-section in Fig. 2, the required area A_N for a certain normal force N can be written as;

$$\frac{N}{f_y} = A_N = R^2(2\alpha+\sin 2\alpha), \quad (18)$$

which expands to;

$$\frac{N}{f_y R^2} = 2\alpha+\sin 2\alpha = 4\alpha-\frac{4}{3}\alpha^3-\mathcal{O}^5 \quad (19)$$

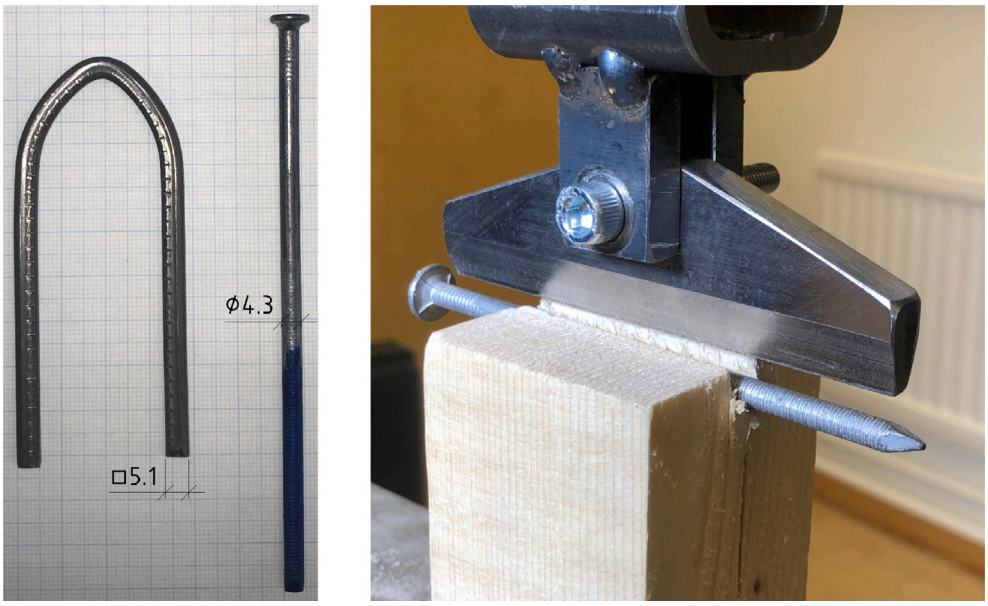

Fig. 4. The U-conn and nail used for the push-out tests (left) and the test setup for embedment tests (right). The fasteners have been photographed on graph millimetre paper.

where the right hand side is the series expansion of the expression including error terms. If the error term is neglected, α is;

$$\alpha = 2\cos\left(\frac{\pi + \arctan\left(\frac{8}{\sqrt{9n^2-1}}\right)}{3}\right) \text{ for } 0 \le n \le \frac{8}{3}, \text{ with } n = \frac{N}{f_y R^2}. \quad (20)$$

The plastic section modulus for the hatched segments in the circular cross-section in Fig. 2 is determined as,

$$\frac{M_y}{f_y} = Z = 4\int_{R\sin\alpha}^{R} y\sqrt{R^2-y^2}\,\mathrm{d}y = \frac{4}{3}R^3\cos^3\alpha. \quad (21)$$

By using (20) in (21), the yield moment as a function of normal force for the circular cross-section can be written as;

$$M_y(N) = f_y\frac{4}{3}R^3\cos^3\left(2\cos\left(\frac{\pi + \arctan\left(\frac{8}{\sqrt{9n^2-1}}\right)}{3}\right)\right). \quad (22)$$

This approximate expression, as well as the exact solution, are normalised against the full yield moment derived with (14) and are plotted in Fig. 3.

3. Material and methods

To determine significant model parameters, tests were conducted on U-shaped connectors (U-conn) in timber boards and on ring-shank nails in glulam beams. The timber boards were collected from a stack of boards in a weatherproof outdoor storage and were all of strength grade C24 M according to [40]. The glulam was of strength grade GL28cs according to [41] and was covered in plastic foil when delivered. Both timber boards and glulam were softwood, Norway spruce (*Picea abies*). When delivered, the moisture content was measured using a resistance moisture metre to about 16% for the timber boards and to about 15% for the glulam. After preparation of tests specimens, they were kept in controlled climate with temperature 22 °C and relative humidity 55%. After a test had been performed, the timber density was determined from the mass and volume of either a timber slice or a cylinder, cut from the vicinity of the fastener. Since the 45 mm thick glulam beam lamellas are of different timber strength grade, cylinders were cut from both lamellas that the nail had penetrated in the withdrawal tests. From the push-out tests, however, only the outer lamella density was determined. Due to the conditioning, the density is assumed to be ρ_{12} and for the push-out test specimens, the moisture content just after the test was determined by oven-drying pieces of timber.

The U-conn:s are cold-drawn steel wire of quadratic cross-section with the nominal side length 5.1 mm, and are presently used in one type of precast TCC element [42,43]. At the precast factory, the wire is cut from rolls by a machine, in which the nail thread is U-shaped. In the same machine, the U-conn:s are pressed into timber boards before being moved further on in the production process. One U-conn is shown in Fig. 4.

The nails used for the push-out tests were ring-shank nails with circular cross-section, see Fig. 4. The nominal diameter and length are 4.2 mm and 130 mm, respectively, with nominal ringed length l_w = 48 mm and tip length l_{tip} = 6.3 mm according to [44]. However, for the nails used in the tests, the diameter and ringed length were measured to 4.3 mm and l_w = 73 mm, respectively. A pneumatic nail gun was used for the assembly. For the embedment tests, however, nails of three different diameters were used.

All tests were performed using an MTS Criterion C45.105 universal testing machine [45] and deformations were measured using MTS AVX-54 video extensometer [46].

Timber embedment strength

For the timber embedment tests, boards with width 47 mm and height 173 or 222 mm were used. The U-conn:s were spaced with an approximate centre-to-centre distance of 90 mm. From the boards, the test specimens were cut out, see Fig. 5. For the nail specimens, boards were prepared with ringed nails driven in the specimen with hammer. After this, they were cut lengthwise to cross-sectional dimension 47 × 48 mm. One end of the specimen was cut to an even and perpendicular surface at a distance of 20d from the nail. Lastly, the test specimen was cut to expose the nail, see Fig. 5. The load was applied by the equipment shown in Fig. 4, with a constant movement of the crosshead of 0.9 mm/min. In the first embedment tests, the tips of the U-conn were blunt since the thread was cut perpendicular to the fastener axis. It was observed that this leads to damage and local crushing of timber when the U-conn:s are pressed into the timber, which can lead to premature splitting failure of the short test specimens. Due to this observation, the embedment strength was also tested using sharpened U-conn:s.

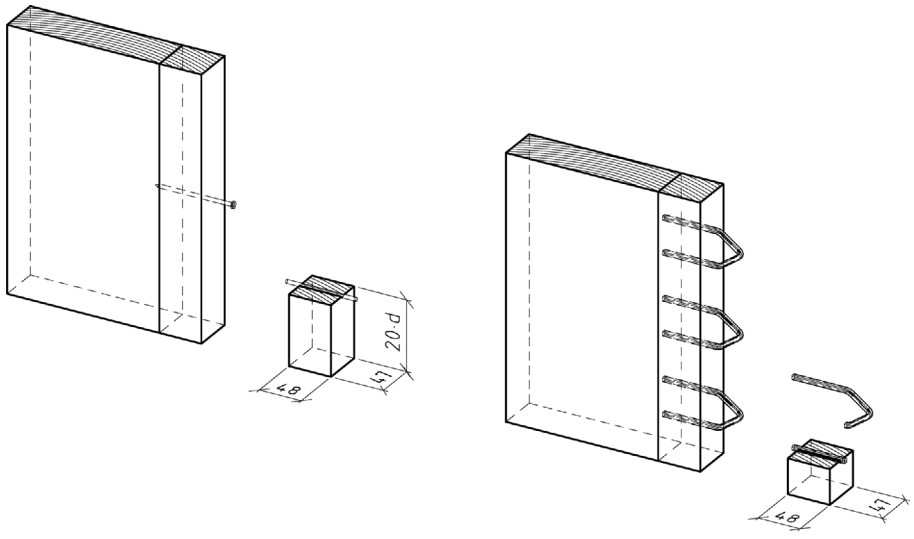

Fig. 5. Embedment test geometry. In the figure, the first illustration on the left side represents how the nails were driven into timber boards and the second illustration from the left shows the dimensions of the cut-out test specimens. The two illustrations on the right side shows the same procedure for the U-conn:s.

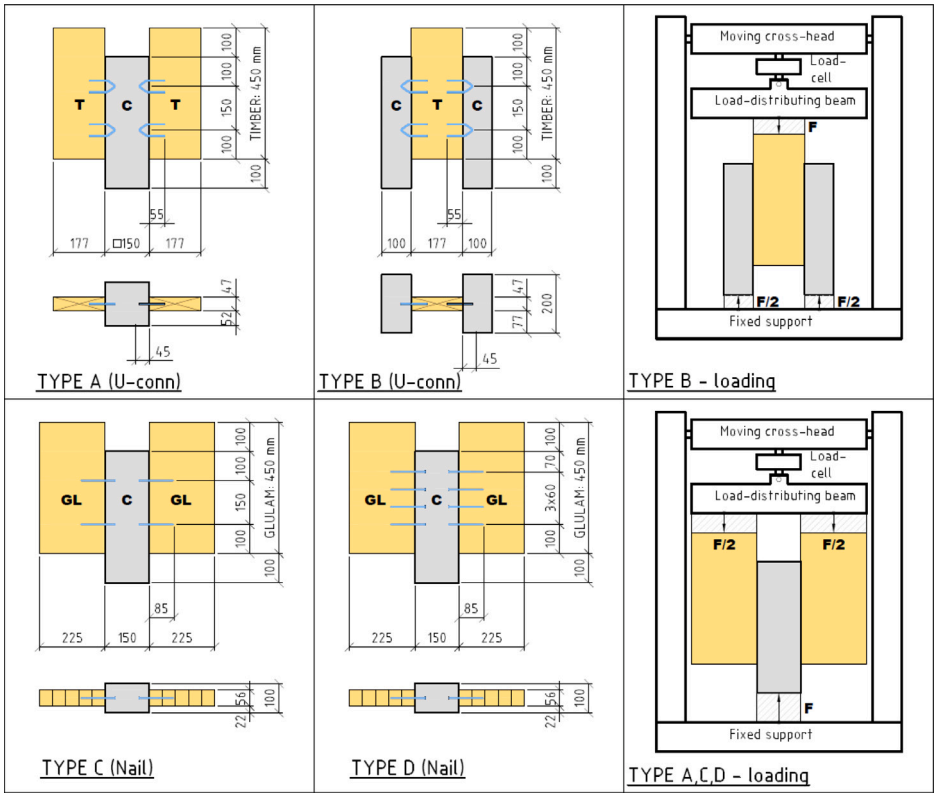

Fig. 6. The test specimens used for push-out tests with U-shaped connectors (top) and nails (bottom). To the right, the load application principle through a moving crosshead and fixed supports is shown for test specimen type B at the top, and types A, C and D at the bottom. C = Concrete, GL = GluLam timber, T = structural Timber, F = Force.

Withdrawal capacity in timber

The withdrawal capacity for U-conn:s in timber boards and nails in glulam are determined from pull-out tests. Before the tests, a line was drawn on the fastener, marking the wood surface, so that the penetration depth l_t could be measured with a caliper after the fastener had been pulled out. The tests were performed with a constant rate of loading, varying between 200–600 N/min for the U-conn:s, and between 2300–3600 N/min for the nails.

Tensile strength of steel

To determine the strength of the fasteners used in the push-out tests, tensile tests were conducted on 100 mm long specimens cut from both fastener types. The specimen was placed in the testing machine with a distance of 50 mm between the grips and the strain was measured between two points 35 mm apart.

Push-out tests

To determine the load-bearing capacity of the connections, push-out tests were performed. For the tests with U-conn:s, sawn timber boards

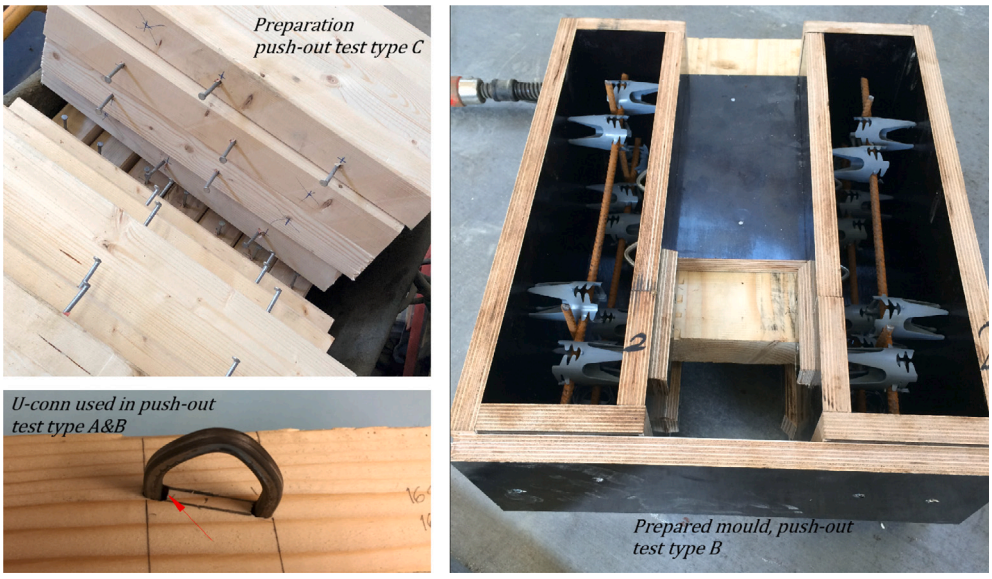

Fig. 7. Preparation of push-out test specimens. Top left are cut glulam beams prepared with nails for test specimens of type C. Bottom left is a detail from one of the U-conn:s pressed into timber, with the arrow indicating the impact on timber from the blunt tip. To the right, a mould prepared with timber beam and reinforcement before casting of test specimen type B is shown. (For interpretation of the references to colour in this figure legend, the reader is referred to the web version of this article.)

Table 1
Concrete recipes used for push-out test specimens, all values are given as [kg/m^3].

Material	Tests A&B	Tests C&D	Comment
Aggregate 0/8	860	870	From natural sand
Aggregate 8/11.2	726	740	From crushed rock
Cement	461	477	CEM II/A-LL 42,5 R[a]
Water	207	209	
Superplasticizer	3.6	–	Sikament HD-100
Superplasticizer	–	2.7	CHRYSO Fluid Premia 205

[a] Swedish *Skövde Byggcement* from Cementa.

(grade C24) were used, while glulam beams (grade GL28) were used for the nail connections. The test specimens with U-conn:s were of two types: concrete as central member and timber as side members (type A) and timber as central member and concrete as side members (type B). The test specimens with nails all had concrete as central member and glulam as side members, but were joined with two nails (type C) or four nails per side (type D). The concrete was reinforced with cut-out parts of mesh reinforcement designated NK500AB-W according to [47], with longitudinal rebars ø8 and transverse rebars ø7. Geometric properties of the different test specimens are given in Fig. 6 and preparation of push-out test specimens is shown in Fig. 7. To assemble the U-conn:s, the aforementioned machine was used, resulting in an angle between the U-conn and the grain angle of the board of approximately 13°, see Fig. 7. The nails were driven into the beams using a pneumatic nail gun, adjusted so that the protruding length to be cast into concrete was 35 mm, see Figs. 6 and 7. The concrete used was from the regular production of precast elements and had a nominal grade of C40/50 according to the factory design mix. The concrete recipes are shown in Table 1. After casting of the concrete the test specimens were covered with a plastic foil until the following day, when the mould was detached. After this the specimens were stored in the production hall for one week before they were taken to the controlled climate, where they were kept until testing. At the time of casting of the concrete for test specimens of type A and B, four cubes with the side 150 mm were also cast. The cubes were kept in steel moulds for one day, hereafter they were stored in water with temperature of 20 °C for four days. After the water storage the cubes were stored in air (20 °C, RH = 65%) until the age 28 days, after which they were tested, using the compression testing machine available at the factory. The results are given in Table 8.

Table 2
Embedment test results for square-sectional nail thread used as U-conn:s. Test U1-U20 are sharpened connectors, while U21–U24 are for blunt ends.

Test spec.	d [mm]	ρ_{12} [kg/m^3]	$f_{h,t}$ [MPa]
U1[a]	5.1	332	14.9
U2[a]	5.1	369	27.4
U3	5.1	370	12.0
U4[a]	5.1	376	18.8
U5[a]	5.1	376	20.1
U6	5.1	380	6.0
U7[a]	5.1	380	16.2
U8[a]	5.1	382	20.0
U9[a]	5.1	390	12.9
U10[a]	5.1	393	16.5
U11	5.1	396	2.7
U12	5.1	396	3.2
U13[a]	5.1	401	18.9
U14	5.1	402	5.9
U15	5.1	402	8.2
U16[a]	5.1	407	26.6
U17	5.1	410	1.4
U18	5.1	481	5.4
U19	5.1	483	5.8
U20	5.1	491	5.9
Sharp U-conn:s	Mean	401	12.4
	CoV	10%	64%
Sharp[a] U-conn:s	Mean	381	19.2
	CoV	5%	24%
U21	5.1	397	1.5
U22	5.1	397	2.6
U23	5.1	402	4.2
U24	5.1	425	4.9
Blunt U-conn:s	Mean	405	3.3
	CoV	3%	47%
All U-conn:s	Mean	402	10.9
	CoV	9%	74%

[a] The values fulfil the failure and deformation criteria discussed above and are used to determine the embedment strength used in the further calculations.

Table 3
Embedment test results for nails.

Test spec.	d [mm]	ρ_{12} [kg/m^3]	$f_{h,t}$ [MPa]
3.0-1	3.0	399	37.3
3.0-2	3.0	410	38.6
3.0-3	3.0	417	35.7
3.0-4	3.0	422	35.4
3.0-5	3.0	433	40.9
Nails, d = 3.0	Mean	416	37.6
	CoV	3%	6%
4.3-1	4.3	396	32.1
4.3-2	4.3	407	30.8
4.3-3	4.3	413	38.2
4.3-4	4.3	425	34.1
4.3-5	4.3	432	34.1
4.3-6	4.3	460	40.8
Nails, d = 4.3	Mean	422	35.0
	CoV	5%	11%
4.7-1	4.7	404	20.7
4.7-2	4.7	440	29.5
4.7-3	4.7	457	15.7
4.7-4	4.7	482	35.7
4.7-5	4.7	515	23.7
Nails, d = 4.7	Mean	460	25.1
	CoV	9%	31%
All Nails	Mean	438	31.3
	CoV	8%	27%

Table 4
Pearson's correlation coefficient (r) between wood density (ρ_{12}) and embedment strength ($f_{h,t}$).

Subsample	$r(\rho_{12}, f_{h,t})$
All tests	0.14
Nails	−0.25
U-conn:s	−0.41
Nails, d = 3.0	0.35
Nails, d = 4.3	0.75
Nails, d = 4.7	0.26
U-conn:s, sharp	−0.45
U-conn:s, sharp[a]	0.24
U-conn:s, blunt	0.80

[a] Indicates the subsample of U-conn:s fulfilling the defined failure and deformation criteria, i.e. the marked test specimens in Table 2.

Table 5
Mean values for embedment strength for the different fastener widths and Pearson's correlation coefficient (r) between diameter (d) and embedment strength ($f_{h,t}$).

d [mm]	$f_{h,t}$ [MPa]
3.0	37.6
4.3	35.0
4.7	25.1
5.1	19.2
$r(d, f_{h,t})$	−0.90

The principle for loading the test specimens is shown furthest to the right in Fig. 6. A first intention was to follow the load protocol according to [48], and the estimated failure-load was determined by tests on five specimens that had been discarded due to knots and finger joints in the timber beams. Thus, the value F_{est} = 25 kN was used in the first ten tests. This method was abandoned, and in the rest of the tests on type A and B the load was applied by a constant crosshead movement of 2 mm/min. For the test specimens of type C and D, the load was also applied by a constant movement of the crosshead. For the first specimen (C1) the rate was 1 mm/min, which was increased to 1.5 mm/min for all subsequent tests.

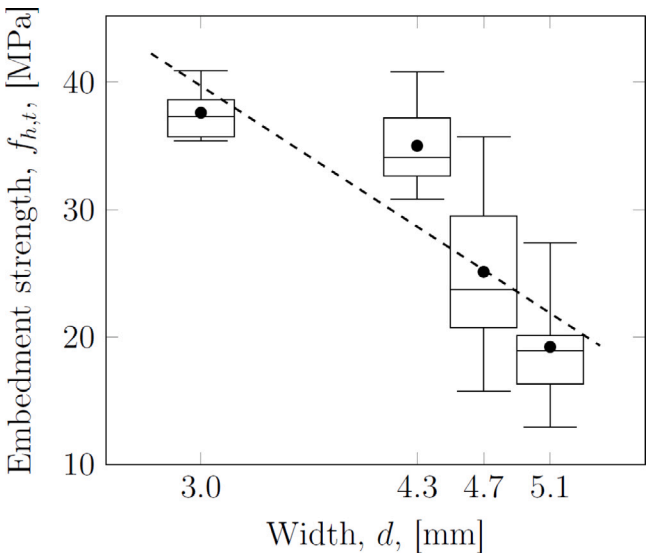

Fig. 8. Embedment strengths for the different widths tested. Solid dots represents the mean embedment strength of each fastener width. The dashed line is the best least square fit of the mean embedment strengths as a function of fastener diameter, i.e. $65.2 - 8.5 \cdot d$.

4. Results and discussion

Timber embedment

From the maximum measured load, P_{max}, the embedment strength was calculated as;

$$f_{h,t} = \frac{P_{max}}{d \cdot l_t} \tag{23}$$

where l_t is the embedment length. The embedment test results are given in Table 2 for the U-conn:s and Table 3 for the different nail diameters. The narrow spacing of U-conn:s resulted in short test specimens which, especially for the blunt U-conn:s, could lead to a splitting failure before a proper embedment strength could be reached. This was especially observed for the U-conn:s with blunt tip. Due to this, it was decided to evaluate the embedment strength for subsamples fulfilling two criteria: (i) the maximum load must be reached before splitting failure, (ii) the deformation at maximum load must be at least 0.5 mm. These failure criteria were chosen since the embedment strength is an important parameter in the calculation models, and since no such splitting failures were observed in the push-out tests, where the U-conn:s were spaced with a greater distance. The correlation between wood density and embedment strength was analysed for the different fasteners, either for the total sample or with the data divided into subsamples. In Table 4 the Pearson's correlation coefficient (r) is given for the different cases. Insignificant correlation was found between timber density ρ_{12} and embedment strength $f_{h,t}$ for the tested timber fasteners, although correlation was observed in some subsamples. The mean value for embedment strength for the three subsamples of nails (d = 3.0, d = 4.3 and d = 4.7) and the sharpened U-conn:s are used to assess the correlation between fastener width and embedment strength. The results are presented in Table 5 and Fig. 8. Between fastener width d and embedment strength $f_{h,t}$, a strong correlation was observed.

Table 6
Withdrawal test results for U-conn:s. Roman numerals denote the board, while Arabic numerals denote the fastener.

Test spec.	ρ_{12} [kg/m^3]	Load rate [N/min]	F_{max} [N]	$l_{t,1}$ [mm]	$l_{t,2}$ [mm]	f_{ax} [MPa]
I-1	301	300	157	57.2	53.8	0.28
I-2	301	300	265	53.8	56.3	0.47
I-3	301	300	255	55.3	55.6	0.45
I-4	383	300	309	54.5	55.4	0.55
I-5	383	300	270	53.2	55.0	0.49
I-6	383	300	404	53.0	55.1	0.73
I-7	383	300	557	57.2	52.9	0.99
II-1	383	300	277	55.8	52.9	0.50
II-2	392	300	409	49.8	57.3	0.75
II-3	384	300	396	55.6	55.6	0.70
II-4	385	300	283	54.4	54.0	0.51
III-1	492	600	352	50.8	53.1	0.66
III-2	492	600	385	54.0	50.0	0.73
III-3	492	550	461	53.3	52.7	0.85
III-4	492	550	313	51.8	52.7	0.59
IV-1	457	300	300	50.5	53.0	0.57
IV-2	457	300	413	52.3	51.1	0.78
IV-3	452	300	472	51.1	52.9	0.89
IV-4	452	300	404	51.1	53.8	0.76
V-1	386	300	442	54.4	53.1	0.81
V-2	383	300	362	52.1	54.2	0.67
V-3	379	300	401	52.4	54.9	0.73
V-4	379	300	397	52.5	54.5	0.73
VI-1	535	300	760	56.5	53.4	1.36
VI-2	519	300	827	55.7	53.8	1.48
VI-3	523	300	699	53.3	55.4	1.26
VII-1	524	300	867	54.8	54.8	1.55
VII-2	526	300	450	56.1	52.8	0.81
VII-3	517	300	835	53.7	55.9	1.49
VIII-1	358	300	742	57.0	56.6	1.28
VIII-2	372	300	567	57.6	55.3	0.98
VIII-3	363	300	889	55.3	57.7	1.54
VIII-4	357	300	816	57.5	55.9	1.41
IX-1	363	300	820	55.2	58.2	1.42
IX-2	402	300	823	55.6	58.2	1.42
IX-3	379	300	413	56.7	56.3	0.72
IX-4	379	300	666	59.4	53.8	1.15
X-1	404	600	457	58.6	55.5	0.79
X-2	404	600	526	58.6	55.5	0.90
XI-1	485	450	774	57.5	56.2	1.33
Mean	418	–	505	54.6	54.6	0.90
CoV	16%	–	42%	4%	3%	40%

Table 7
Withdrawal test results for nails. Roman numerals denote the glulam beam, while Arabic numerals denote the fastener. The withdrawal parameter, f_{ax} is determined from the ringed length l_w = 73 mm.

Test spec.	$\rho_{12,out}$ [kg/m^3]	$\rho_{12,in}$ [kg/m^3]	Load rate [N/min]	F_{max} [N]	l_t [mm]	f_{ax} [MPa]
XII-1	480	408	3600	3301	86.3	10.8
XII-2	480	408	3600	3477	86.3	11.3
XII-3	480	408	3600	2559	87.5	8.3
XII-4	480	408	3600	4353	86.3	14.2
XIII-1	457	351	3600	3447	85.6	11.2
XIII-2	457	351	3600	3275	85.4	10.7
XIII-3	457	351	3600	3053	85.9	10.0
XIII-4	457	351	3600	2963	86.4	9.7
XIV-1	473	359	3600	3434	84.6	11.2
XIV-2	473	359	3600	2311	86.1	7.5
XIV-3	473	359	3600	3418	85.1	11.1
XIV-4	473	359	3600	2855	84.4	9.3
XV-1	494	495	3600	4202	83.6	13.7
XV-2	494	495	3600	5267	84.1	17.2
XV-3	563	495	3600	4205	82.6	13.7
XV-4	563	495	3600	5315	82.2	17.2
XVI-1	476	361	3600	3056	86.2	10.0
XVI-2	476	361	3600	3307	86.6	10.8
XVI-3	476	361	3600	2844	87.4	9.3
XVI-4	476	361	3600	2950	87.0	9.6
XVII-1	474	377	2300	3278	85.4	10.7
XVII-2	474	377	2300	3053	83.8	10.0
XVII-3	474	377	2300	3018	84.0	9.8
XVII-4	474	377	2300	3062	84.6	10.0
XVIII-1	431	395	2300	2709	86.3	8.8
XVIII-2	431	395	2300	3546	86.3	11.6
XVIII-3	431	395	2300	2801	86.1	9.1
XVIII-4	431	395	2300	2869	86.7	9.4
Mean	474	392	–	3355	85.4	10.9
CoV	6%	12%	–	21%	2%	21%

Table 8
Compressive strength of tested concrete cubes from the casting of test specimens of type A and B to the left, and steel strength from tensile tests on the different fastener types to the right. The concrete cylinder strength is calculated according to [49] as $0.8 f_{cc,cube}$.

$f_{cc,cube}$ [MPa]	$f_{cc,cyl}$ [MPa]	$f_{y,U-conn}$ [MPa]	$f_{y,nail}$ [MPa]
56.6	45.3	473	625
57.8	46.2	507	609
57.8	46.2	467	624
58.2	46.6	436	622
–	–	–	623
57.6	46.1	471	621
1%	1%	6%	1%

Withdrawal tests

The withdrawal parameter was calculated from the maximum load, F_{max}, as;

$$f_{ax} = \frac{F_{max}}{d \cdot l_w} \tag{24}$$

where l_w is the withdrawal length of the fastener. For the U-conn:s l_w was taken as the sum of penetration depths of the two shanks, while the ringed length l_w = 73 mm was used for the nails. In Tables 6 and 7 detailed test data for the U-conn:s and for the nails are given. The correlation between the withdrawal parameter and wood density was determined, resulting in r = 0.38 for the U-conn:s and r = 0.64 and r = 0.77 for the nails, using the density of the outer and inner lamella, respectively.

Steel strength

From the measured force, the engineering stress was calculated. The tensile strength for the U-conn:s was determined as the stress resulting in 0.2% plastic strain, while the yield strength for the nails were determined visually from stress–strain diagrams. The results are given in Table 8.

Hinge location and deformation angle

After the test, the timber members were cut to study the deformed shape of the fasteners and the location, x_t, of the plastic hinge on the timber side. The concrete was not split to study the corresponding distance, x_c, but it was noted that the fastener had bent on some distance from the concrete surface, with minor scaling of the concrete. The fasteners were photographed and the subsequent studies were done using CAD software. The distance x_t was defined as the distance from the concrete surface to the intersection of the centre lines of the unbent fastener shanks, while the bending angle was defined either as φ_1 or φ_2, see Fig. 9. Detailed data from the measurements are given in Tables 9, 10, 12 and 13. For the U-conn:s, the hinge location on the timber side was measured for each test specimen and the correlation between the hinge location x_t and the timber density ρ_{12} and the moisture content ω was investigated. This was done for the whole sample of tested U-conn:s as well as for the subsamples of type A and type B separately. The results are shown in Table 11. Insignificant correlation was found between the plastic hinge location x_t and timber density or moisture content ω. For the round nails the location was measured on 12 nails from specimen type C and 32 nails from type D, see Tables 9–10. Unfortunately, it was not registered from which test specimen the measured nails were originating. As a consequence, the correlation between hinge location and other measured parameters could not be determined.

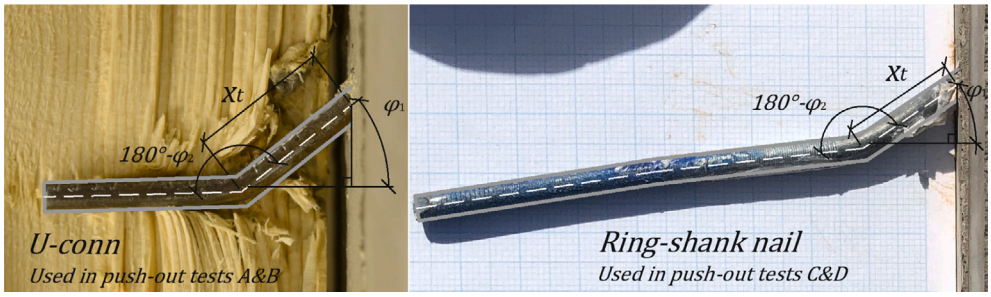

Fig. 9. Definition of plastic hinge location and the angles φ_1 and φ_2 in test specimen of type A and B (left), and type C and D (right). The photograph to the right is taken with graph millimetre paper in the background, and the scale is the same for both pictures.

Table 9
Measured plastic hinge locations x_t and bending angle φ for the nails in test specimens of type C.

	Type C (nails)					
	Nail 1 (upper)			Nail 2 (lower)		
	x_t [mm]	φ_1 [°]	φ_2 [°]	x_t [mm]	φ_1 [°]	φ_2 [°]
	24.9	26.7	23.0	23.4	27.4	13.3
	23.3	30.1	22.9	21.4	30.0	13.0
	21.9	25.7	23.3	21.2	29.3	12.1
	19.5	33.7	27.3	20.6	28.6	13.9
	23.8	18.3	14.4	21.8	18.2	11.9
	21.9	17.0	24.3	21.5	22.8	19.1
Mean	22.6	25.3	22.5	21.7	26.1	13.9
CoV	8%	26%	19%	4%	18%	19%
	$x_{t,mean}$ = 22.1 mm (CoV = 7%) $\varphi_{1,mean}$ = 25.7° (CoV = 21%) $\varphi_{2,mean}$ = 18.2° (CoV = 31%)					

The test specimens with U-conn:s (type A and B) were all deformed to a total crosshead movement of 25 mm, and the same deformation for the tests with ring-shank nails (type C and D) was 15 mm. The failure load, however, was reached at a crosshead movement typically between 10–20 mm for the U-conn:s and 5–10 mm for the nails. Thus, large plastic deformations of the fasteners have taken place after the maximum load was reached. Thus, these bending angles are not measures to determine the hinge location when maximum load is reached, nor load-bearing capacity of the fasteners.

Load-bearing capacity

The load-bearing capacities for the tests are given in Tables 12–14 and was determined by dividing the maximum measured load by the number of fastener shanks in a test specimen, where U-conn:s have two shanks and nails one of course. The correlation between the maximum load F_{max} and the minimum, maximum and mean values of the density ρ_{12} and the moisture content ω were also determined and results are given in Table 15. Insignificant correlation was found between the load-bearing capacity and the timber density ρ_{12} or the moisture content ω for the tested fasteners, although correlation was observed in some subsamples.

5. Model vs. experiment

The hinge locations as well as the load-bearing capacities are calculated with the theoretical models using the mean values of the evaluated material parameters above. The calculated values are compared to the corresponding values from the push-out tests. The input parameters used in the calculations are given in Table 16. To determine the embedment strength of concrete, the relation $f_{h,c} = \kappa \cdot f_{cc,cyl}$ is used, wherein $f_{cc,cyl}$ is the mean compressive cylinder strength from Table 8 and κ = 4.6 according to [19].

Hinge location

In the undeformed state, the hinge location is calculated using (5). For the deformed state, the hinge location is calculated with (10) for two cases, one with M_y according to (13) and (14), and one with reduced M_y by using the axial force from (8) as the normal force in (17) or (22). The results of the calculations as hinge location vs. deformation angle are shown in Fig. 10.

How the mechanical response changes from purely elastic to full plastic with an increasing bending angle is described in [35]. The bending angle for full plasticity is here approximated, using this method, to $\varphi \approx 6°$ for the U-conn:s with quadratic cross-section, and to $\varphi \approx 9°$ for the nails with circular cross-section. These angles are used to determine the location of the plastic hinge in the deformed state. The results are shown and compared to the experimental values in Table 17.

Load-bearing capacity

When the location of the plastic hinge is known, the load-bearing capacity F_{DEF} can be calculated with (12), using the input parameters given in Table 16. This was done and the results are shown in Fig. 11.

For the model with the fasteners in deformed state, the angle for full plasticity ($\varphi = 6°$ and $\varphi = 9°$ for quadratic and circular cross-section, respectively) are used in (12) to determine the load-bearing capacity. Furthermore, the load-bearing capacity is determined for the case of undeformed fastener using (6) and (7). The results are shown and compared to the experimental values in Table 18. It should be noted that the calculated load for the U-conn:s is per fastener shank, assuming that the failure load for one U-conn is determined by multiplication of this load by 2. This is a simplified assumption, and in many cases a reduction of the load-bearing capacity is evident, cf. staples with low crown-grain angle in [25]. If a reduction of this kind would be taken into account, the difference between experimental and theoretical values would increase.

The models are also compared by calculation of the load-bearing capacity as functions of the timber density of the test specimens with nails in Table 14. The timber embedment strength is calculated according to [52] as $f_{h,t} = 0.09 \cdot \rho_{12} \cdot d^{-0.36}$. A function for the withdrawal strength as function of density is evaluated from the relation between withdrawal parameter and density of the outer lamella in Table 7, as $f_{ax} = 0.049 \cdot \rho_{12} - 12.25$. These strength parameters, input from Table 16 and the deformation angle $\varphi = 9°$, are used in the models. The load is calculated using the density for each side of the specimen in Table 14, and is then summed over the number of fasteners on each side. The results are shown in Fig. 12. The correlation between experimental and calculated values is good for all models, but the model derived from the deformed state shows higher accuracy when compared with the experimentally determined maximum load. To evaluate the models further, the mean squared error (MSE) was calculated, and results are given in Table 19.

Table 10
Measured plastic hinge locations x_t and bending angle φ for the nails in test specimens of type D.

	Type D (nails)											
	Nail 1 (upper)			Nail 2			Nail 3			Nail 4 (lower)		
	x_t [mm]	φ_1 [°]	φ_2 [°]	x_t [mm]	φ_1 [°]	φ_2 [°]	x_t [mm]	φ_1 [°]	φ_2 [°]	x_t [mm]	φ_1 [°]	φ_2 [°]
	18.6	26.6	26.6	19.5	31.8	24.7	17.8	30.8	25.2	19.4	29.1	18.4
	20.5	30.0	21.7	22.3	29.2	18.3	24.1	23.0	14.1	23.1	28.1	13.5
	20.2	26.1	28.4	23.3	24.0	21.2	21.9	26.6	19.1	25.1	28.8	10.7
	20.8	26.2	26.2	21.6	23.3	22.5	22.3	26.9	19.9	17.9	23.0	10.0
	18.3	26.6	25.5	18.5	30.5	25.6	18.3	33.4	24.3	17.6	31.3	22.0
	16.6	26.3	22.6	19.6	29.0	25.6	19.4	25.9	19.1	17.1	31.4	19.9
	24.2	26.0	22.3	23.0	26.6	22.3	23.6	25.3	16.7	23.5	24.1	11.5
	21.5	26.9	24.2	21.3	27.7	22.7	23.0	26.8	18.6	22.9	27.1	15.8
Mean	20.1	26.8	24.7	21.1	27.8	22.9	21.3	27.3	19.6	20.8	27.9	15.2
CoV	11%	5%	10%	12%	11%	11%	11%	12%	19%	10%	11%	30%

$x_{t,mean}$ = 20.8 mm (CoV = 11%)
$\varphi_{1,mean}$ = 27.5° (CoV = 10%)
$\varphi_{2,mean}$ = 20.6° (CoV = 24%)

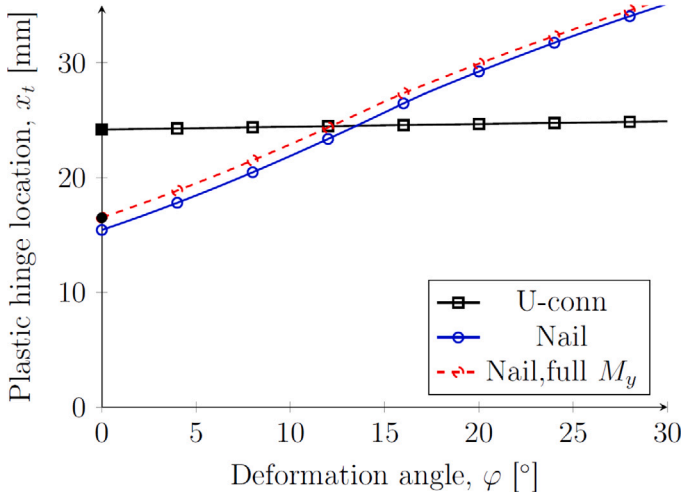

Fig. 10. The plastic hinge location x_t for an increasing value of the bending angle φ. The solid line curves are determined with the yield moment from (17) and (22) for the U-conn and the nail, respectively, while the dashed curved is determined with the full yield moment in (10). The black square and dot markers on the ordinate represents the value for x_t determined with the model in undeformed state, i.e. (5) for the U-conn and nail, respectively.

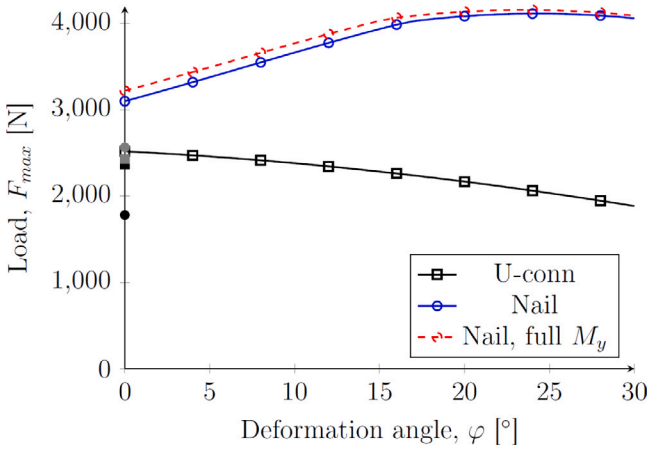

Fig. 11. The load-bearing capacity, F_{max}, for an increasing value of the deformation angle φ. The curves are determined with (12) with the yield moment from (17) and (22) for the U-conn and the nail, respectively. Input parameters for the calculations are given in Table 16. The black square and dot markers on the ordinate represents the load-bearing capacity determined in the undeformed state with (6) for the U-conn and nail, respectively, while the corresponding gray markers represents these values with added rope-effect according to the EYM determined with (7).

Table 11
Pearson's correlation coefficient (r) between the measured value for x_t and timber density ρ_{12} and moisture content ω for the U-conn:s (test specimen type A and B).

Sample	$r(x_t, \rho_{12})$	$r(x_t, \omega)$
All U-conn:s	−0.26	−0.20
Type A (U-conn:s)	−0.09	−0.11
Type B (U-conn:s)	−0.35	0.04

6. Conclusions

The equilibrium models usually adopted to determine the load-bearing capacity for timber to timber connections can, as shown here, be used also for connections between timber and concrete components. When compared to experimental data, the theoretical model derived from the undeformed state including rope-effect (EYM) showed similar results to the model derived from the deformed state (DEF) for the U-shaped connectors, made of cold-drawn steel wire of quadratic cross-section, having low withdrawal capacity (F_{EYM}/F_{exp} = 75% and F_{DEF}/F_{exp} = 75%). When the U-conn:s are pressed into the timber, it has a significant impact and crushing is evident. This is shown both in the withdrawal and embedment tests, where the U-conn:s show high

Table 12
Timber density ρ_{12}, moisture content ω, plastic hinge location x_t and deformation angle φ, and maximum load per fastener shank F_{max} for test specimen type A. For x_t, the index 1 and 2 are the upper and lower U-conn as depicted in Fig. 6. Where there are two numbers presented, both shanks of the U-conn have been measured. It should be noted that the maximum load F_{max} is per fastener shank, i.e. the load-bearing capacity per U-conn is twice this load.

Type A (U-conn:s)										
			U-conn 1 (upper)			U-conn 1 (lower)				
Test spec.	ρ_{12} [kg/m^3]	ω [%]	x_t [mm]	φ_1 [°]	φ_2 [°]	x_t [mm]	φ_1 [°]	φ_2 [°]	Load app.	F_{max} [N]
A1-R	529	12.2	23.3	44.0	58.9	23.7	35.7	42.9	1	3227
A1-L	456	11.9	29.7	45.8	24.7	25.7	49.4	16.2		
A2-R	414	11.1	–	–	–	24.0	41.2	33.5	2	3569
A2-L	391	11.4	23.3/24.0	57.5/43.3	22.4/38.8	24.3	43.5	28.2		
A3-R	372	11.8	28.5	52.1	16.0	24.1	46.5	20.8	1	2938
A3-L	392	11.7	25.9	43.1	37.7	22.2	39.6	38.4		
A4-R	453	11.0	26.2	46.4	23.7	26.5	39.3	37.1	2	3102
A4-L	455	11.4	23.3	50.4	36.4	27.1	46.4	23.6		
A5-R	410	12.1	–	–	–	–	–	–	1	3104
A5-L	452	11.9	–	–	–	–	–	–		
A6-R	433	10.7	23.6	49.3	34.9	26.3	58.6	20.2	2	3193
A6-L	454	10.7	25.1	41.3	25.6	26.0	54.9	24.8		
A7-R	466	10.5	23.6	40.7	31.3	22.4	40.8	39.2	1	2978
A7-L	470	11.0	23.7	46.5	36.4	25.9	34.7	22.4		
A8-R	449	11.2	27.7	43.0	18.7	27.0	40.3	25.6	2	2909
A8-L	471	11.3	24.7	48.0	19.3	23.7	44.0	17.0		
A9-R	514	11.3	26.0	35.7	21.7	28.1	43.3	18.1	1	2902
A9-L	458	11.2	25.2	37.9	36.5	27.7/30.6	42.4/46.1	19.6/31.1		
A10-R	535	11.7	23.9/23.6	–	–	26.0	–	–	2	3334
A10-L	404	10.5	30.3	62.6	8.3	25.9/26.4	–	–		
Mean	449	11.3	25.3	46.3	28.9	25.7	43.9	27.0	–	3126
CoV	10%	5%	9%	15%	41%	8%	14%	32%	–	7%

$x_{t,mean}$ = 25.5 mm (CoV = 8%)
$\varphi_{1,mean}$ = 45.1° (CoV = 14%)
$\varphi_{2,mean}$ = 27.9° (CoV = 36%)

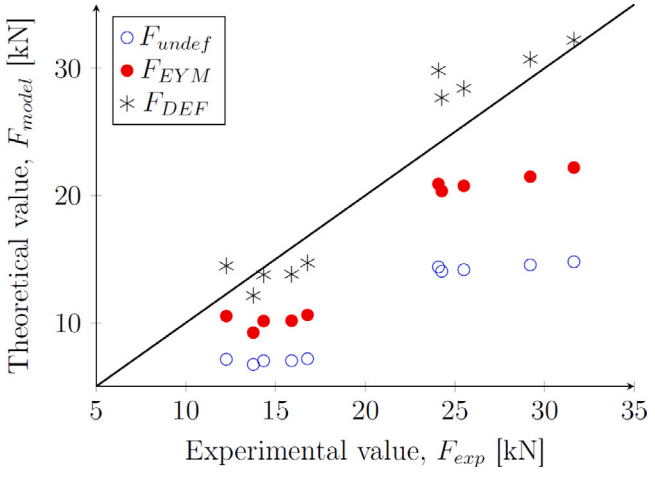

Fig. 12. The load per test specimen of type C and D plotted against the load determined with the different theoretical models.

variation. It is likely so that this also has an impact on the wood between the shanks. If this would have been taken into account and the calculated values were reduced, the difference between them and the experimental values would be even higher. For the ring-shank nails, when compared to experimental data, all models showed good correlation. However, the model derived from equilibrium in the deformed state of the fastener showed better precision than the model derived from the initial and undeformed configuration (F_{EYM}/F_{exp} = 75% and F_{DEF}/F_{exp} = 103%), with lower mean square error (MSE = 30.9 for F_{EYM} and MSE = 7.2 for F_{DEF}). The models derived from the undeformed state were consequently showing conservative values, while the model derived from the deformed state overestimated the load-bearing capacity in six out of ten specimens. This could be an indication that the used deformation angle φ = 9° is too high. Future studies could be focused on how to determine a relevant deformation angle for the model. It is also noted that the model tends to overestimate the load-bearing capacity for test specimens with a higher number of fasteners, thus future studies could investigate the impact of number of, and distance between, fasteners in both the push-out test and TCC connection.

Furthermore, due to the low axial capacity of the U-conn:s, the theoretical models for both the undeformed and the deformed states give similar results for the plastic hinge location ($x_{t,undef.}/x_{t,exp}$ = 97% and $x_{t,DEF}/x_{t,exp}$ = 98%). This can be explained by setting q_{ax} to zero in (10), which then will become (5). For the ring-shank nails, however, also the prediction of the location of the plastic hinge shows a better fit when the model derived from the deformed configuration is used ($x_{t,undef.}/x_{t,exp}$ = 78% and $x_{t,DEF}/x_{t,exp}$ = 100%).

It should be noted that, if (12) is used for a bending angle of φ = 0°, it will have contributions to the load-bearing capacity from both friction and axial force, which is impossible. Thus, for a bending angle of φ = 0° it is more correct to use only Eq. (6).

In the push-out tests, the test specimens were loaded to a pre-chosen deformation, which lead to large plastic deformations in fasteners after that the maximum load was reached. To be able to determine at what angle of fastener bending the capacity is reached, a method to study the fastener should be discussed.

When correlation was determined between strength parameters and other measurements, the correlation between strength and density and strength and moisture content usually was insignificant or low. It should be noted, however, that the tests have involved only two

Table 13
Timber density ρ_{12} and moisture content ω, plastic hinge location x_t and deformation angle φ, and maximum load per fastener shank F_{max} for test specimen type B. Load app. 1 = EN 26891, 2 = constant crosshead movement (2 mm/min). For x_t, the index 1 and 2 are the upper and lower U-conn as depicted in Fig. 6. Where there are two numbers presented, both shanks of the U-conn have been measured. It should be noted that the maximum load F_{max} is per fastener shank, i.e. the load-bearing capacity per U-conn is twice this load.

Type B (U-conn:s)										
			U-conn 1 (upper)			U-conn 1 (lower)				
Test spec.	ρ_{12} [kg/m^3]	ω [%]	x_t [mm]	φ_1 [°]	φ_2 [°]	x_t [mm]	φ_1 [°]	φ_2 [°]	Load app.	F_{max} [N]
B1-R	450	11.8	–	–	–	–	–	–	1	3795
B1-L	457	12.1	–	–	–	–	–	–		
B2-R	437	12.0	31.0	39.2	4.1	27.0	39.3	7.4	2	2710
B2-L	419	11.9	30.4	40.7	6.0	27.4	38.0	11.2		
B3-R	362	11.6	–	–	–	–	–	–	1	2848
B3-L	348	11.8	–	–	–	–	–	–		
B4-R	442	11.7	26.3	39.1	20.1	23.5	39.2	32.2	2	3337
B4-L	422	12.3	22.8	43.7	15.6	26.9	54.0	35.0		
B5-R	411	12.3	26.5	42.5	18.3	26.3	68.0	23.1	1	3258
B5-L	358	11.8	28.1	50.1	35.8	25.6/25.2	51.4/48.3	28.0/29.9		
B6-R	424	11.6	23.8/22.3	47.5/60.9	30.4/60.9	27.3	51.0	23.6	2	3397
B6-L	407	11.8	19.4/17.9	53.1/69.2	3.7/58.7	22.9	48.1	15.2		
B7-R	534	12.2	19.5	37.2	40.6	23.4	45.3	32.9	1	3696
B7-L	534	12.4	23.6	46.0	47.7	25.0	52.5	24.2		
B8-R	489	12.3	24.3	54.9	17.0	24.7	55.5	21.4	2	3185
B8-L	515	12.0	23.8	60.2	25.2	27.3	61.6	38.1		
B9-R	515	11.7	19.8	36.3	39.9	21.5	39.9	33.6	1	3560
B9-L	516	12.1	21.7	29.8	36.0	24.3	39.0	37.7		
B10-R	517	12.4	23.0	48.7	50.7	24.1	55.3	26.2	2	3988
B10-L	504	12.1	21.0	34.4	21.2	20.9	42.9	34.6		
Mean	423	12.0	23.6	46.3	29.6	24.9	48.8	26.7	–	3377
CoV	13%	2%	16%	22%	61%	8%	18%	34%	–	12%

$x_{t,mean}$ = 24.2 mm (CoV = 12%)
$\varphi_{1,mean}$ = 47.5° (CoV = 20%)
$\varphi_{2,mean}$ = 28.2° (CoV = 50%)

Table 14
Timber density ρ_{12} and moisture content ω, number of nails n and maximum load per nails F_{max} for test specimen type C and D.

	ρ_{12} [kg/m^3]	ω [%]	n	F_{max} [N]
C1-R	470	11.0	4	3063
C1-L	473	10.9		
C2-R	492	11.0	4	4195
C2-L	463	11.2		
C3-R	464	10.7	4	3583
C3-L	445	11.3		
C4-R	421	11.1	4	3439
C4-L	407	11.3		
C5-R	451	11.2	4	3973
C5-L	460	11.2		
D1-R	471	10.5	8	3033
D1-L	441	11.2		
D2-R	483	10.7	8	3187
D2-L	447	10.9		
D3-R	525	11.3	8	3954
D3-L	500	10.7		
D4-R	530	10.8	8	3650
D4-L	458	10.8		
D5-R	429	10.9	8	3010
D5-L	537	10.7		
Mean	468	11.0	–	3509
CoV	8%	2%	–	12%

Table 15
Pearson's correlation coefficient (r) between the measured maximum load F_{max} per fastener shank and density ρ_{12} and moisture content ω of the timber.

Sample	$r(F_{max}, \rho_{12})$			$r(F_{max}, \omega)$		
	max	min	mean	max	min	mean
All	0.25	0.37	0.33	0.08	0.04	0.06
U-conn:s	0.32	0.37	0.37	0.43	0.29	0.37
Nails	0.05	0.44	0.24	0.43	0.51	0.61
A (U-conn)	−0.01	−0.42	−0.20	0.12	−0.15	0.03
B (U-conn)	0.58	0.57	0.58	0.52	0.39	0.49
C (nail)	0.38	0.12	0.26	0.41	0.36	0.52
D (nail)	0.45	0.94	0.87	0.29	0.52	0.70

Table 16
Input parameters for the calculations for the two types of fasteners tested.

Variable	Name	Unit	U-conn.	Nail	Comment
Width	d	mm	5.1	4.3[a]	–
Embedment length, timber	l_t	mm	55	100	–
Embedment length, concrete	l_c	mm	35	30	–
Yield strength	f_y	MPa	471	621	From tests
Yield moment	M_y	N mm	15 620	8229	–
Withdrawal parameter	f_{ax}	MPa	0.9	10.9	From tests
Concrete strength	$f_{cc,cyl}$	MPa	46	46	From tests
Embedment strength, timber	$f_{h,t}$	N/mm	19.2	25.1	From tests
Embedment strength, concrete	$f_{h,c}$	N/mm	212	212	From [19]
Friction coeff., wood-concrete	μ_{wc}	–	0.4	0.4	From [50]
Friction coeff., wood-steel	μ_{ws}	–	0.1	0.1	From [51]
Limiting constant	A	–	25%	50%	From [37]
Withdrawal length	l_w	mm	55	73[a]	–

[a] The diameter and ringed length are measured and differ from values given in the DoP [44].

Table 17
Experimental and theoretical values for the plastic hinge location.

U-conn., dist. [mm]		$x_t/x_{t,exp}$
$x_{t,exp,mean}$	24.9	–
$x_{t,undef.}$	24.2	97%
$x_{t,DEF,\varphi=6°}$	24.3	98%
Nails, dist. [mm]		$x_t/x_{t,exp}$
$x_{t,exp,mean}$	21.2	–
$x_{t,undef.}$	16.5	78%
$x_{t,DEF,\varphi=9°}$	21.2	100%

Table 18
Experimental and theoretical values for the load-bearing capacity.

U-conn., load [N]		F/F_{exp}
$F_{exp,mean}$	3251	–
$F_{undef.}$	2369	73%
F_{EYM}	2432	75%
$F_{DEF,\varphi=6°}$	2446	75%
Nails, load [N]		F/F_{exp}
$F_{exp,mean}$	3509	–
$F_{undef.}$	1782	51%
F_{EYM}	2638	75%
$F_{DEF,\varphi=9°}$	3611	103%

Table 19
The Pearson's correlation coefficient (r) and mean square error (MSE) between the maximum load determined with the different models and the experimentally determined ditto.

Model	r	MSE
F_{undef}	0.95	112.6
F_{EYM}	0.95	30.9
F_{DEF}	0.96	7.2

strength grades of timber, with a narrow density span. Furthermore, all test specimens were stored and conditioned in the same climate.

CRediT authorship contribution statement

Johan Pyykkö: Writing – review & editing, Writing – original draft, Visualization, Validation, Software, Resources, Project administration, Methodology, Investigation, Funding acquisition, Formal analysis, Data curation, Conceptualization. **Staffan Svensson:** Writing – review & editing, Supervision.

Declaration of competing interest

The authors declare the following financial interests/personal relationships which may be considered as potential competing interests: Johan Pyykkö reports financial support was provided by Gunnar Ivarsons Stiftelse, GIS. Johan Pyykkö reports financial support was provided by Hedareds Sand & Betong AB. Staffan Svensson reports financial support was provided by Gunnar Ivarsons Stiftelse, GIS. Johan Pyykkö reports a relationship with Hedareds Sand & Betong AB that includes: employment. Johan Pyykkö reports a relationship with Gunnar Ivarsons Stiftelse, GIS that includes: funding grants. Staffan Svensson reports a relationship with Gunnar Ivarsons Stiftelse, GIS that includes: funding grants. If there are other authors, they declare that they have no known competing financial interests or personal relationships that could have appeared to influence the work reported in this paper.

Data availability

Data will be made available on request.

Acknowledgements

The authors would like to thank Gunnar Ivarson's Foundation (Gunnar Ivarsons Stiftelse, GIS) and Hedareds Sand & Betong AB (Heda) for the financial support that made this work possible. We would also like to thank our colleague Dr. Mats Desaix for helping us find analytic expressions for the roots of the cubic equation in (19).

References

[1] Ceccotti A. Composite concrete-timber structures. Prog Struct Eng Mater 2002;4:264–75, eprint: https://onlinelibrary.wiley.com/doi/pdf/10.1002/pse.126. https://onlinelibrary.wiley.com/doi/abs/10.1002/pse.126.

[2] Zhang X, Hu X, Gong H, Zhang J, Lv Z, Hong W. Experimental study on the impact sound insulation of cross laminated timber and timber-concrete composite floors. Appl Acoust 2020;161:107173, https://www.sciencedirect.com/science/article/pii/S0003682X19309545.

[3] Parmanen J, Sipari P, Uosukainen S. Sound insulation of multi-storey houses: Summary of impact sound insulation. In: VTT technical research centre of Finland. VTT PUBLICATIONS 377; 1999, http://www.inf.vtt.fi/pdf/.

[4] Casagrande D, Giongo I, Pederzolli F, Franciosi A, Piazza M. Analytical, numerical and experimental assessment of vibration performance in timber floors. Eng Struct 2018;168:748–58, https://www.sciencedirect.com/science/article/pii/S0141029617323052.

[5] Xie Z, Hu X, Du H, Zhang X. Vibration behavior of timber-concrete composite floors under human-induced excitation. J Build Eng 2020;32:101744, https://www.sciencedirect.com/science/article/pii/S2352710220333775.

[6] Marshall J, Granello G, Palermo A. Vibration performance of timber-concrete-composite floors: a case study. SESOC J 2020;33(1):33–46.

[7] Martins C, Skinner J, Bregulla J, Harris R, Paine K, Walker P, Dias AMPG. Concrete upgrade to improve the vibration response of timber floors. Proc Inst Civ Eng (ICE) - Struct Build 2014;167:559–68. http://dx.doi.org/10.1680/stbu.13.00057, eprint: https://doi.org/10.1680/stbu.13.00057.

[8] Lukaszewska E. Development of prefabricated timber-concrete composite floors (doctoral thesis) (Ph.D. thesis), Luleå, Sweden: Luleå University of Technology; 2009, http://urn.kb.se/resolve?urn=urn:nbn:se:ltu:diva-18042.

[9] Plüss Y, Zwicky D. A case study on the eco-balance of a timber-concrete composite structure in comparison to other construction methods. In: Proceedings of the 1st concrete innovation conference (CIC), 11-13 June 2014, Oslo, Norway. Oslo, Norway: Concrete innovation centre, Norsk Betongforening; 2014.

[10] Basaglia B, Lewis K, Shrestha R, Crews K. A comparative life cycle assessment approach of two innovative long span timber floors with its reinforced concrete equivalent in an Australian context. In: Proceedings of the second international conference on performance-based and life-cycle structural engineering. PLSE 2015, Brisbane, Australia: School of Civil Engineering, The University of Queensland; 2015, p. 1433–42.

[11] Yeoh D, Fragiacomo M, Franceschi MD, Boon KH. State of the art on timber-concrete composite structures: Literature review. J Struct Eng 2011;137(10):1085–95.

[12] Dias AMPG, Schänzlin J, Dietsch P. Design of timber-concrete composite structures: A state-of-the-art report by COST actionFP 1402/WG 4. Achen, Germany: Shaker Verlag GmbH; 2018.

[13] Dias AMPG, Lopes SMR, vana de Kuilen J-W, Cruz HMP. Load-carrying capacity of timber-concrete joints with Dowel-Type fasteners. J Struct Eng 2007;133(5):720–7.

[14] Johansen KW. Theory of timber connections, vol. 9, Zürich, Switzerland: Publications from International Association for Bridge and Structural Engineering; 1949, p. 249–62.

[15] Larsen HJ. K. W.Johansen's nail tests, vol. 48, Aalborg, Denmark: Bygningsstatiske Meddelelser; 1977.

[16] Möller T. En ny metod för beräkning av spikförband. Gothenburg, Sweden: Chalmers Tekniska Högskolas Handlingar: Transactions of Chalmers University of Technology; 1951.

[17] Larsen HJ. The yield load of bolted and nailed joints. In: Egerup AR, Larsen HJ, Riberholt H, Sørensen E, editors. Papers presented at IUFRO-V, international union of forestry research organization, division V, congress 1973. København, Danmark: Structural Research Laboratory, Technical University of Denmark; 1974, p. 16–31.

[18] Meyer A. Die tragfähigkeit von nagelverbindungen bei statischer belastung. Holz Roh-und Werkstoff 1957;15:96–109.

[19] Rasmussen BH. Betonindstøbte Tværbelastede Boltes og Dornes Bæreevne, vol. 34, København, Danmark: Bygningsstatiske Meddelelser, Dansk Selskab for Bygningsstatik; 1963, p. 39–55.

[20] Miloš M, Predrag P, Todor V, Andrija Z, Ivan N. Design of nailed timber-concrete composite joint according to eurocode and FEA. Facta Univ Ser: Archit Civil Eng 2022;20(3):301–11.

[21] Tako D, Denouwe DD, Messan A, Bouchaïr A. Experimental and numerical investigations of timber-concrete connections using variant forms of rebars. Eng Struct 2023;291:116441, https://www.sciencedirect.com/science/article/pii/S0141029623008568.
[22] Khorsandnia N, Valipour HR, Crews K. Experimental and analytical investigation of short-term behaviour of LVL-concrete composite connections and beams. Constr Build Mater 2012;37:229–38, https://www.sciencedirect.com/science/article/pii/S0950061812004916.
[23] Oudjene M, Meghlat E, Ait-Aider H, Lardeur P, Khelifa M, Batoz J-L. Finite element modelling of the nonlinear load-slip behaviour of full-scale timber-to-concrete composite T-shaped beams. Compos Struct 2018;196:117–26, https://www.sciencedirect.com/science/article/pii/S0263822318310869.
[24] Seim W, Schick M, Waschkowitz T. The European yield model (EYM) for laterally loaded timber connections with smooth nails. Wood Mater Sci Eng 2022;17:965–78. http://dx.doi.org/10.1080/17480272.2021.1983870, eprint: https://doi.org/10.1080/17480272.2021.1983870.
[25] EN 1995-1-1:2004. Eurocode 5: Design of timber structures - Part 1-1: General - Common rules and rules for buildings. Brussels, Belgium: European Commitee for Standardization (CEN); 2004.
[26] CEN/TS 19103:2022. Eurocode 5: Design of timber structures - structural design of timber-concrete composite structures - common rules and rules for buildings. European Commitee for Standardization (CEN); 2021.
[27] Dias AMPG, vana de Kuilen J-W, Cruz HMP. Mechanical properties of timber-concrete joints made with steel dowels. In: Proceedings of the 36th CIB-W18 meeting. Colorado, USA: Internationas Council for Research Innovation in Building Construction; 2003.
[28] Kavaliauskas S, Kvedaras AK, Valiunas B. Mechanical behaviour of timber-to-concrete connections with inclined screws. J Civ Eng Manag 2007;13(3):193–9.
[29] Berardinucci B, di Nino S, Gregori A, Fragiacomo M. Mechanical behavior of timber-concrete connections with inclined screws. Int J Comput Methods Exp Meas 2017;5(6):807–20.
[30] Johari IB, Mohd Snin MAB, Senin SFB. Screw connection systems in timber-concrete composite structures: A literature review. Tehn Vjesnik 2023;vol. 30(4):1336–46.
[31] Gelfi P, Giuriani E, Marini A. Stud shear connection design for composite concrete slab and wood beams. J Struct Eng 2002;128:1544–50.
[32] Manojlović D, Rašeta A, Vukobratović V, Čeh A, Kozarić L, Jovanović Đ, Starčev-Ćurčin A. Simulation of load-slip capacity of timber-concrete connections with dowel-type fasteners. Buildings 2023;13. https://www.mdpi.com/2075-5309/13/5/1171.
[33] Pyykkö J, Svensson S. Deformations of slender dowel-type fasteners in timber-concrete composite connections. Determination of load-slip curves from mechanical equilibrium. In: Proceedings of the 20th international conference on experimental mechanics. Porto, Portugal: INEGI-FEUP; 2023, p. 20172.
[34] Kuipers J, vana der Put TA. Betrachtungen zum bruchmechanismus von nagelverbindungen. In: Ingenieurholzbau in Forschung und Praxis: Karl Möhler gewidmet. 1982, p. 99–106.
[35] Svensson S, Munch-Andersen J. Theory of timber connections with slender dowel type fasteners. Wood Mater Sci Eng 2018;13:7–15. http://dx.doi.org/10.1080/17480272.2016.1226382, eprint: https://doi.org/10.1080/17480272.2016.1226382.
[36] Pyykkö J, Svensson S. Slender dowel-type fasteners in timber-concrete composite connections. Determination of load-bearing capacity in deformed state. In: Proceedings of the 20th international conference on experimental mechanics. Porto, Portugal: INEGI-FEUP; 2023, p. 19906.
[37] Larsen HJ. In: Munch-Andersen J, editor. CIB - w18 timber structures - a review of meetings 1-43. Part 6: Essays. Lyngby, Denmark: Danish Timber Information; 2011, p. 40–50.
[38] Sandhaas C, Görlacher R. In: Sandhaas C, Munch-Andersen J, Dietsch P, editors. Design of connections in timber structures: a state-of-the-art report by COST action FP1402 / WG3. Aachen, Germany: Shaker Verlag GmbH; 2018, p. 61–74.
[39] Svensson S, Wittsten J. Modelling plastic behavior of slender dowel type fastener in three point bending tests. In: Proceedings of the 20th international conference on experimental mechanics. Porto, Portugal: INEGI-FEUP; 2023, p. 20085.
[40] EN 15497:2014. Structural finger jointed solid timber - Performance requirements and minimum production requirements. Brussels, Belgium: European Commitee for Standardization (CEN); 2014.
[41] EN 14080:2013. Timber structures - Glued laminated timber and glued solid timber - Requirements. Brussels, Belgium: European Commitee for Standardization (CEN); 2013.
[42] Pyykkö J, Ogrin A, Hozjan T. Behaviour of timber-concrete beams exposed to natural fire. In: Proceedings of the 2nd international fire safety symposium. IFireSS 2017, Naples, Italy; 2017, p. 101.
[43] Pyykkö J. Prediction of moisture state in prefabricated timber-concrete composite elements subjected to varying climate in early age. In: Proceedings of the engineering mechanics institute (EMI) conference 2018. Cambbridge, MA, USA: ASCE, Massachusetts Institute of Technology; 2018.
[44] Paslode. Declaration of performance, DoP 001/2013 (version 9). Middelfart, Denmark: Paslode; 2022.
[45] MTS Systems. MTS criterion series 40 electromechanical universal test systems. Minnesota, USA: MTS Systems Corporation; 2023, (read at: https://www.mts.com/-/media/materials/pdfs/brochures/mts-criterion-test-system-brochure.pdf).
[46] MTS Systems. MTS Advantage Video Extensometer brochure. Minnesota, USA: MTS Systems Corporation; 2015.
[47] SS 212540:2014. Product specification for SS-EN 10080:2005 - Steel for the reinforcement of concrete - Weldable reinforcing steel - Technical delivery conditions for bars, coils, welded fabric and lattice girders. Stockholm, Sweden: Swedish Standards Institute (SIS); 2013.
[48] EN 26891:1991. Timber structures - Joints made with mechanical fasteners - General principles for the determination of strength and deformation characteristics. Brussels, Belgium: European Commitee for Standardization (CEN); 1991.
[49] EN 1992-1-1:2005. Eurocode 2: Design of concrete structures - Part 1-1: General rules and rules for buildings. Brussels, Belgium: European Commitee for Standardization (CEN); 2005.
[50] EN 1995-2:2004. Eurocode 5:Design of timber structures - Part 2: Bridges. Brussels, Belgium: European Commitee for Standardization (CEN); 2004.
[51] Sjödin J, Serrano E, Enquist B. An experimental and numerical study of the effect of friction in single dowel joints. Holz Roh-und Werkstoff 2008;363–72, https://doi.org/10.1007/s00107-008-0267-z.
[52] Whale L, Smith I, Hilson B. Characteristic properties of nailed and bolted joints under short-term lateral load, part 4 - the influence of testing mode and fastener diameter upon embedment test data. J Inst Wood Sci 1989;11:156–61.